Time–electric field superposition in electrically activated polypropylene/layered silicate nanocomposites

Jun Uk Park [a], Yang Suk Choi [a], Kwang Soo Cho [b], Do Hoon Kim [a,1], Kyung Hyun Ahn [a,*], Seung Jong Lee [a]

[a] *School of Chemical and Biological Engineering, Seoul National University, Seoul 151-744, South Korea*
[b] *Department of Polymer Science, Kyungpook National University, Daegu 702-701, South Korea*

Abstract

This study investigated the microstructural evolution of PP/clay nanocomposites under electric field. The storage modulus, which is a kind of mirror of the microstructure, increases while an electric field (both AC and DC) is applied. It was found that time and the electric field strength can be superposed to yield a single mastercurve that is independent of the type and strength of the electric field. In addition, the shift factor scaled differently according to the field type. The SAXS and TEM data revealed that the AC field induces the microstructural evolution of the nanocomposites toward an exfoliated structure, while the DC field induces the alignment of silicate layers. In a DC field, the alignment process occurs as a result of dielectrophoretic motion. However, in an AC field, dielectric relaxation analysis showed that an exfoliation process arises as a result of the breakup of the charge balance.
© 2006 Elsevier Ltd. All rights reserved.

Keywords: Electric field; PP/clay nanocomposite; Rheology

1. Introduction

The potential use of inorganic nanoparticles as additives to improve the polymer performance has attracted a great deal of attention. With a smaller loading content, the nanoparticles improve the polymer performance over conventional fillers. The use of nanoparticles facilitates the development of new processes and reduces the weight of the composite. The small size of nanoparticles gives the nanocomposites outstanding properties such as diffusion-barrier properties [1], reduced flammability [2], etc. which cannot be achieved with conventional microcomposites.

In the case of polymer-layered silicate (PLS) nanocomposites, the large contact area between the polymer and the nanoelement enhances the stress transfer. The enhancement of the polymer performance depends on the microstructure of the PLS nanocomposites, which are normally classified into two types: (1) intercalated hybrids, in which a part of the polymer chain intrudes between the silicate layers to form a well-ordered multilayer with an alternating polymer and clay layers; and (2) exfoliated hybrids, where the silicate layers are fully separated and dispersed homogeneously throughout the polymer matrix. The former may be thought of as a system with limited solubility compared with the latter, which shows practically unlimited solubility that allows the effective stress transfer between nanoelements [3]. Accordingly, previous challenging attempts have focused on fabricating nanocomposites with exfoliated hybrids that are known to be superior to those with intercalated hybrids or conventional microcomposites.

The usual methods for preparing polymer nanocomposites involve (1) in situ polymerization [1,4–7], (2) solution blending [8,9], (3) direct melt mixing [10–12] with various polymer systems ranging from thermoplastics to thermosets. However, the commercial application of the first two methods has limitations because they suffer from the selection of suitable solvent, high cost, environmental problems, etc. On the other hand, direct melt mixing is a promising approach because it is more versatile for commercial polymers and less harmful to the environment due to the absence of solvent. Although direct melt mixing has great potential as a non-solvent process having good compatibility with conventional

---

polymer-processing equipment, non-polar polymers such as polypropylene require a compatibilizer [12] to form an exfoliated hybrid.

Previously, it was reported that an electric field is effective for exfoliating clays in polypropylene melts [13]. This study reports the effects of AC and DC electric fields on the clays in polypropylene melts, with particular focus on their similarity and difference. The rheological properties as a function of the duration time of the applied electric field were normalized to show a similarity between the effects of AC and DC fields. It was found that the normalized storage modulus can be superposed onto a single master curve irrespective of the type and strength of the electric field (AC or DC) when it is plotted against the reduced time, which is the time normalized to the characteristic time (or the shift factor) that is a function of the electric field. Although AC and DC form a single master curve in the plot of the normalized modulus versus reduced time, they have different effects on clay, as evidenced by transmission electron microscopy (TEM), in situ synchrotron small angle X-ray scattering (SAXS) and parameter analysis, which characterizes the storage modulus as a function of the duration time of the applied electric field.

2. Experimental section

The polypropylene (PP, M_w:127,000, M_n:13,000) used in this study was purchased from PolyMirae Corp.(Grade: HP562T). The dimethyl hydrogenated-tallow ammonium modified montmorillonite (Cloisite® 20A), which was prepared by ion-exchanging sodium montmorillonite with alkyl ammonium cations, was a kind gift from Southern Clay Products Inc. and was used as received. Melt compounding of the PP/clay hybrid was performed in an intensive internal mixer (Haake Rheocord 90) at 180 °C for 10 min after clay feeding with a 50 rpm rotor speed. The clay and polymer samples were dried in a vacuum oven at 80 °C for 24 h before compounding and the weight fraction of the Cloisite® 20A in the nanocomposites was fixed to 5 wt%.

A rheometrics mechanical spectrometer (RMS 800) was used to determine the rheological performance of the PP/clay nanocomposites under an AC or DC field with a 25 mm parallel plate fixture and 1 mm gap thickness. All the rheological measurements were carried out at a fixed temperature of 180 °C under a nitrogen gas flow. The time sweep tests for monitoring the electric field effect were performed at a frequency of 1 rad/s and a strain of 10%, which is in the linear region at 180 °C.

The time-resolved synchrotron-SAXS measurements were performed at the 4C2 beam line in the Pohang accelerator light source (PALS, Korea), which consists of a 2 GeV linear accelerator (LINAC), a storage ring, a Si(111) double crystal monochromator, various ion chambers, and a two-dimensional CCD camera with a 1024×1024 pixel resolution. The photon energy was set to 5.5 keV. The SAXS patterns were recorded using a two-dimensional camera located 22 cm from the sample. The detector can monitor up to 50 frames at a rate of 40 s per frame. An AC field of 1 kV/mm and 60 Hz, and a DC field of 1 kV/mm were applied between the plates using a
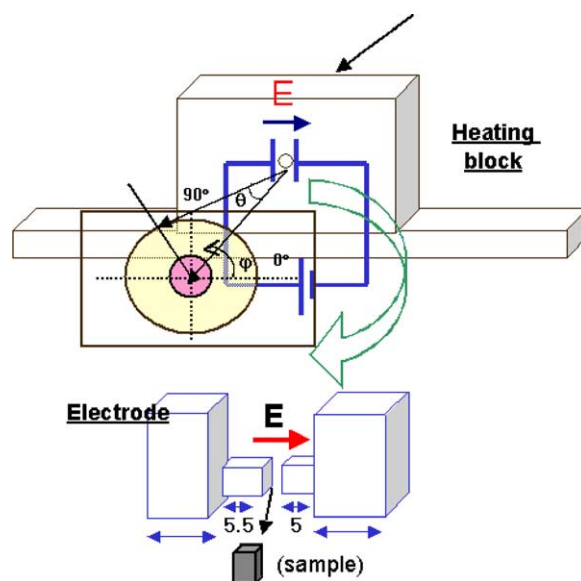
Fig. 1. Schematic diagram of the apparatus for in situ 2D synchrotron-SAXS measurement.

function generator (Tektronix AFG 310) and a high voltage amplifier (Trek 677B). The copper electrode has a 1.5 mm gap, a height of 5 mm and a width of 1 mm. An electric field was applied perpendicular to the direction of the X-ray beam. No leakage current was detected. Fig. 1 shows a schematic of the apparatus.

In order to investigate the morphological change under electric field, TEM was conducted using a Jeol 2010F at an acceleration voltage of 200 kV. The samples for TEM were obtained by rapid quenching after the rheological measurements under an AC field of 1 kV/mm and 60 Hz for 3300 s and a DC field of 1 kV/mm for 1000 s, respectively. Obtained samples were sectioned by cryo-microtoming because of a flexible characteristic of PP matrix.

Dielectric relaxation analysis was carried out to understand the origin of exfoliation in an AC field. A dielectric analyzer, DEA 2970 (TA instruments, Inc.) was used to estimate the dielectric properties of the electrically activated PP/clay nanocomposites under the isothermal condition of 190 °C. Dielectric properties were measured at a frequency range between 0.1 and 10^5 Hz. The samples for dielectric relaxation analysis are subsequently referred to as HP (Neat PP), HPC (PP with 5 wt% of clay), HPCA (treated under AC electric field), and HPCD (treated under DC electric field).

3. Results and discussion

It was reported that an AC electric field can induce the structural evolution of PP/clay nanocomposites, showing a tendency toward exfoliation [13]. This study investigated the different morphological changes in the silicate layers according to the type of electric field (AC and DC). The structural change in the nanocomposite could be detected easily by the rheological measurements on account of its high sensitivity to the microstructural changes in nanocomposites [14–17].

The storage modulus (G') of the nanocomposite under electric fields (AC and DC) was measured as a function of the duration of the applied field because the reinforcing effect of nanocomposites is more pronounced in this property than in the others [18–20]. Fig. 2 shows that the storage modulus normalized to the modulus without the electric field increases with increasing duration time, representing the morphological evolution, finally reaching a constant value after a long duration time indicating the termination of the microstructural change [21]. The change in melt viscosity was from 460 to 620 Pas, which was not as significant as G'. G' increases to its saturation value faster with increasing electric field. When DC field is applied, its saturation value shows little dependence on the field strength. In contrast, the saturation value is strongly dependent on the field strength in AC field, which suggests a different mechanism in their microstructural evolution. This behavior can be expressed by the following equation for both AC and DC fields with any field strength

$$\frac{G'(t)-G'_0}{G'_i-G'_0} = 1-\exp\left(-\frac{t}{\lambda}\right), \quad (1)$$

where G'_0 is the initial modulus before applying the electric field, G'_i is the modulus at infinite time after applying the electric field, λ is the characteristic time (or retardation time), which depends on the material, temperature and electric field. The solid lines in Fig. 2 show the results of non-linear regression of Eq. (1). In all cases, the effect of the electric field on G' can be well predicted using the above equation regardless of the types of electric field. As indicated by the arrows marked in Fig. 2, rapid microstructural evolution is observed with increasing field strength. This means that the increase in the electric field can reduce the exposure time necessary for the desired G' value. This also means that the electric field strength and duration time of the applied electric field is mutually complementary. When the normalized modulus is plotted as a function of the reduced time (t/λ), all the data collapse to a single master curve, which is independent of the type and strength of the electric field (Fig. 3). This shows a universal relationship between the electric field and the exposure time in the microstructural evolution of polymer layered silicate nanocomposites. This is similar to the time–temperature superposition (TTS) [22], and might be called time–electric field superposition (TES). A similar universal behavior has also been observed in the linear viscoelasticity of monodisperse linear polymers [23] in which the shift factor is a function of the power of the reduced molecular weight. This was also observed in the universal scaling of weakly aggregating colloidal particle systems [24] where the shift factors are a function of the volume fraction of the colloidal particles (their vertical shift factor is a function of the power of the horizontal shift factor). This means that the observation of microstructural evolution through the storage modulus can be described by a simple relationship eventhough there may be complex mechanisms according to types of electrical filed. Although AC and DC share with common master curves, the observation of the storage modulus shows that AC and DC should have different effects on the storage modulus because, G'_i and λ have different dependence on field strength according to types of field.

With the assistance of Eq. (1), the parameters, G'_i and λ can be determined as a function of electric field. Fig. 4 shows the characteristic time λ under the AC and DC fields as a function
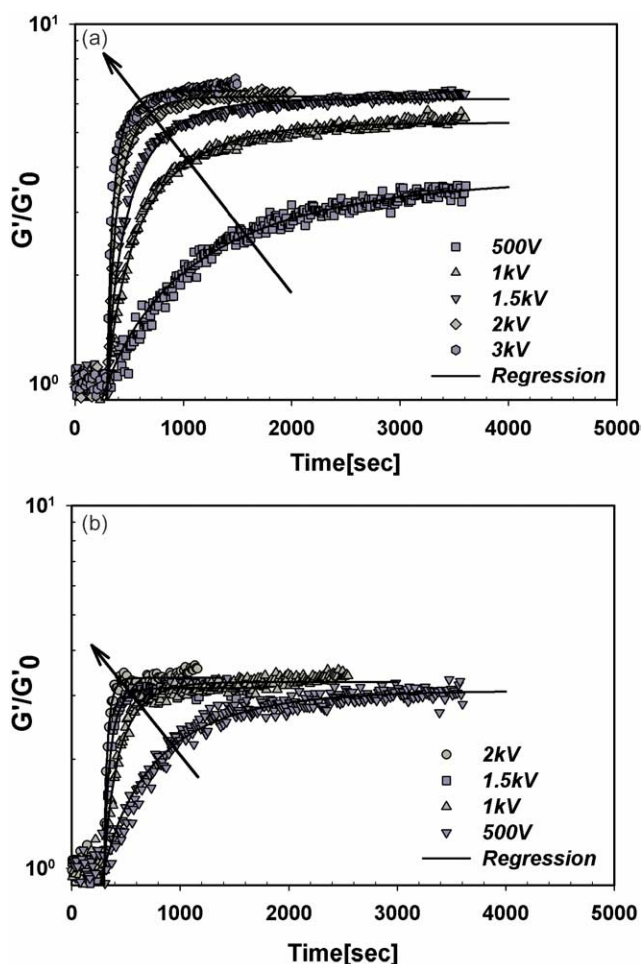
Fig. 2. Growth of storage modulus with the electric field strength (a) AC (b) DC (AC 1 kV–60 Hz and DC 1 kV were applied at 300 s, respectively).
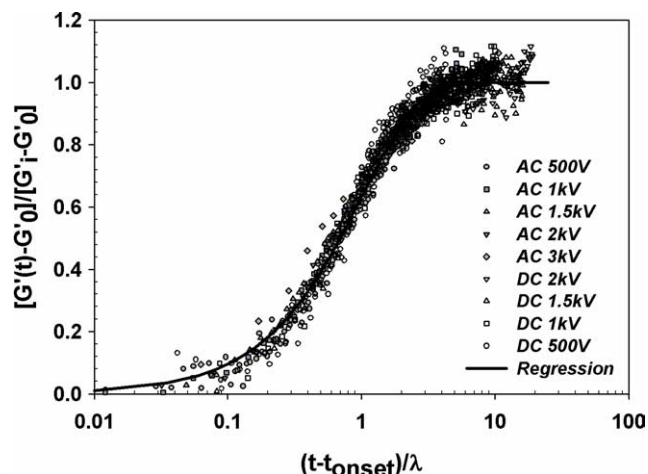
Fig. 3. Normalized modulus ($[G'(t)-G'_0]/[G'_i-G'_0]$) versus reduced time (($t-t_{\text{onset}}$)/λ) ($t_{\text{onset}}=300$ s).
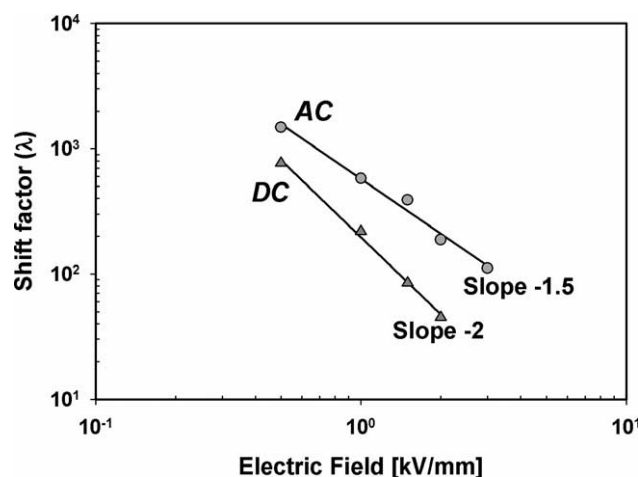
Fig. 4. Shift factor (λ) as a function of the electric field strength.

of electric field strength. It should be noted that λ scales with the power of the electric field strength, but has different exponents (AC, -1.5 and DC, -2) according to the types of electric field. Differences between AC and DC also can be observed when the modulus enhancement (G_i'/G_0') is plotted against the electric field. In the case of AC, G_i'/G_0' increases with increasing electric field to saturation value while it is almost constant in the case of DC (Fig. 5). The parameter analysis shows that AC and DC have different effects on the PP/clay nanocomposites. These different effects suggest different morphological evolution.

SAXS measurement was performed to analyze both the morphological changes and the physical meaning of the difference in the rheological measurements. In situ SAXS was used as a real-time measurement of the microstructural change in the nanocomposites under electric fields, because a conventional lab-scale X-ray scattering device has limitations on account of low intensity and long exposure time required.

Fig. 6 shows the scattering patterns of PP/clay nanocomposites under AC and DC fields. The isotropic ring pattern that represents the random dispersion state of the silicate layers is changed into two different patterns with time under the electric field (both AC
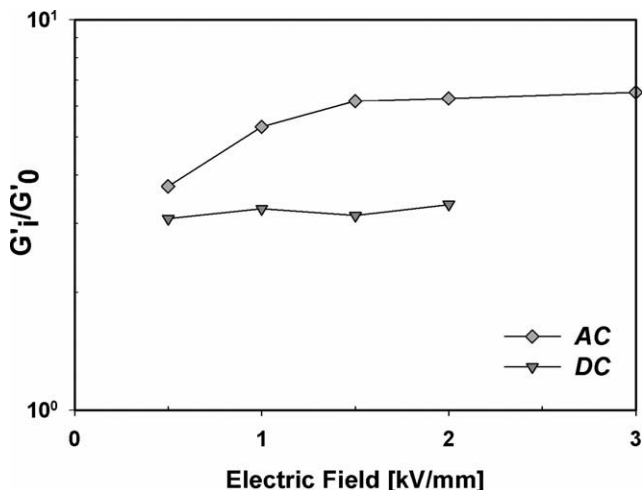
Fig. 5. G_i'/G_0' as a function of the electric field strength.

and DC). After applying AC field of 1 kV/mm and 60 Hz, the isotropic ring pattern shrinks toward the center of the scattered ring and its intensity decreases (Fig. 6(a)). This indicates a tendency toward exfoliation, as shown in the previous studies [13] with 1D XRD data. On the other hand, the alignment of silicate layers parallel to the direction of the DC field (1 kV/mm) is observed, as indicated by the enhanced intensity along the meridian and the concurrent decrease in intensity along the equator of the X-ray scattering pattern (Fig. 6(b)). Fig. 7 shows the change of basal d_{001} spacing for PP/clay nanocomposites in AC and DC fields. While interlayer spacing increases continuously due to the exfoliation in AC field, only a slight change is observed in DC field. Furthermore, the difference in structural evolution between AC and DC is more pronounced in the azimuthal scan at $q=0.2113$ in Fig. 8. The intensity without a noticeable peak in AC field decreases with the duration time as indicated by arrows indicating the trend toward exfoliation with no alignment (Fig. 8(a)). Small peaks at 530 and 1060 s, which go away after 1315 s, are probably from small amount of alignment during the sample molding and loading at melting state. On the other hand, in DC field, two distinct peaks are observed at 90 and 270°. As time goes on, the peak intensity is getting stronger with the concurrent decrease of peak distribution clearly representing a preferential orientation of the clay parallel to the electric field direction. Therefore, the scattering patterns and their analysis indicate that AC induces exfoliation and DC induces the alignment of clay particles and no exfoliation. SAXS provided clear evidence showing the difference between the effects of AC and DC fields. These SAXS results can be supported by TEM images.

Figs. 9 and 10 show the morphological differences according to the electric field types. As can be seen in Figs. 9(d) and 10(d), layers are tightly stacked and randomly dispersed, before electric field application. However, under AC field, the destruction of layer-stacking is observed throughout PP matrix (Fig. 9). Although low-magnification TEM (Fig. 9(c)) shows the presence of micrometer-size clay-rich particles, at higher magnification, TEM images (Fig. 9(a) and (b)) reveal that the initial particles are exfoliated to some degree into very thin and also into single clay plates. In some regions, complete exfoliation into a single plate or a few plate tactoids is observed. In comparison to Figs. 9 and 10 displays TEM micrographs of the PP/clay nanocomposite after DC application. Some stacks or tactoids of silicate layers are clearly observed as thick dark lines along the electric field direction (Fig. 10(a)). The higher-magnification TEM images (Fig. 10(b) and (c)) show that well-ordered tactoids are oriented without increase of inter-layer spacing.

By combining the rheological, SAXS and TEM results, these findings can be summarized as follows:

[1] The increase in the storage modulus can be differentiated by two processes: alignment and exfoliation of clay particles.
[2] The speed of the alignment depends on the strength of the DC field according to $\lambda \propto E^{-2}$.
[3] The speed of the exfoliation depends on the strength of the AC field according to $\lambda \propto E^{-1.5}$.

(a) **AC electric field of 1 kV/mm and 60 Hz**

Initial state | 530 sec

1 060 sec | 1 315 sec

1 845 sec | 2 385 sec

(b) **DC electric field of 1 kV/mm**

Initial state | 53 sec

159 sec | 212 sec

265 sec | 318 sec
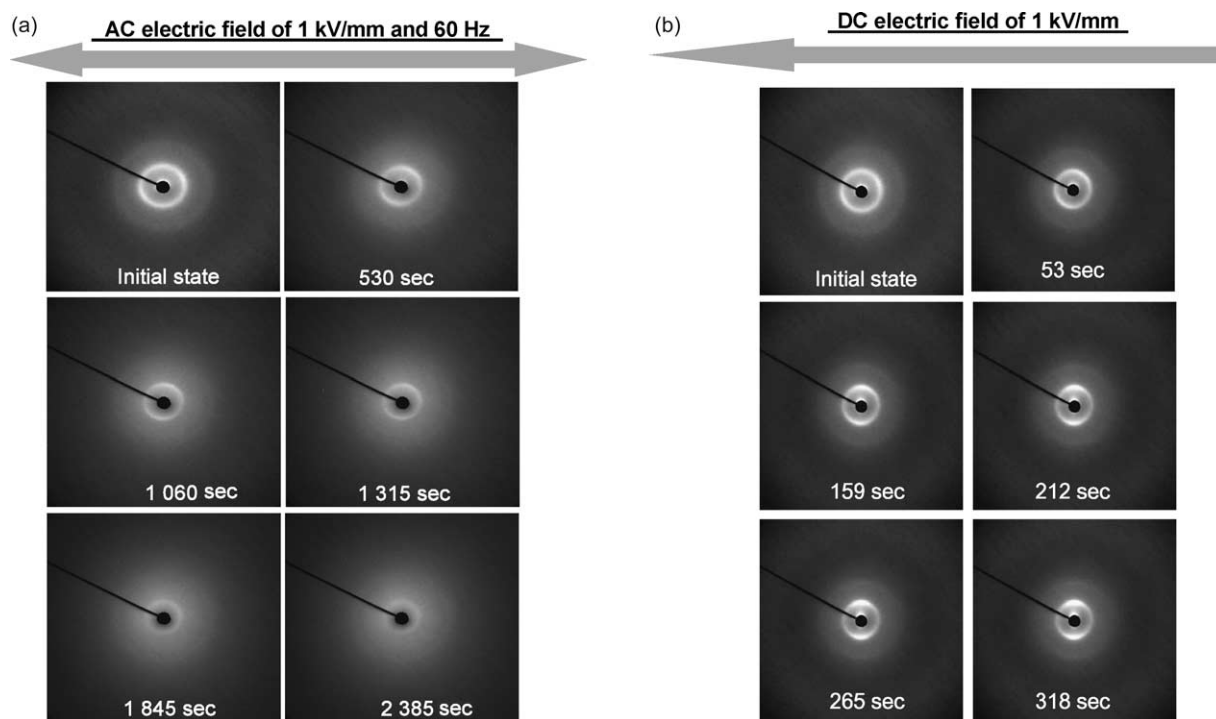
Fig. 6. Time series of in situ 2D SAXS images under (a) AC field and (b) DC field.

[4] The completion of alignment is independent of the strength of the DC field.

[5] The completion of exfoliation depends on the strength of the AC field.

The main questions to be answered are 'why the storage modulus under different electric fields can be described by a single equation such as Eq. (1) and what is the origin of the difference?'. The following reasoning was used to answer these questions.

It is assumed that the completion of nanostructure evolution (alignment and exfoliation) is represented by $\Delta G'_\infty \equiv G'_i - G'_0$, because the modulus of the particulate composites depends on the distribution of filler particles as well as their loading content. Consider a particulate composite system such that the loading content of filler, ϕ is fixed and the distribution of filler particles is random. We can control the orientation of the filler particles. The degree of alignment determines the modulus of the composite and there is the maximum degree of alignment where all filler particles have the same orientation. Because DC field causes alignment of clay particles, it can be concluded that the maximum alignment of clay particles is the equilibrium structure of the composite, which would be established at infinitely long duration time of DC field. It suggests that the modulus at infinite time under DC field is independent of the DC field strength (Fig. 5), while the speed of the alignment depends on the DC field strength. Because the viscosity of the polymer melt is high, it is difficult to expect a significant change in the configuration of the clay particles (position of each clay particle), which are not yet nanoparticles but layer-stacking or tactoids.

The exfoliation of clay particles causes an increase in the number of separate silicate layers. If AC field has an effect on the nanocomposite, i.e. the exfoliation of the clay particles, then there must be equilibrium in the degree of exfoliation for a given strength of AC field. The degree of exfoliation determines the G'_i value, which is a function of the AC field strength (Fig. 5). This is analogous to a chemical reaction, in which the speed of the reaction depends on the AC field strength. This analogy suggests that $\Delta G'_\infty$ represents the equilibration constant of the exfoliation reaction and λ represents the inverse of the kinetic constant of the reaction.

Consider the validity of the TES in more quantitative way. Let the degree of evolution of the nanostructure be x, which is a function of time and the electric field strength. Then, the
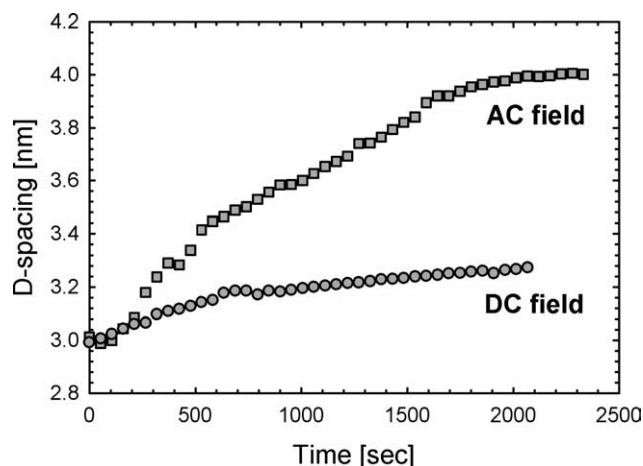
Fig. 7. The change of basal spacing d_{001} under electric fields.
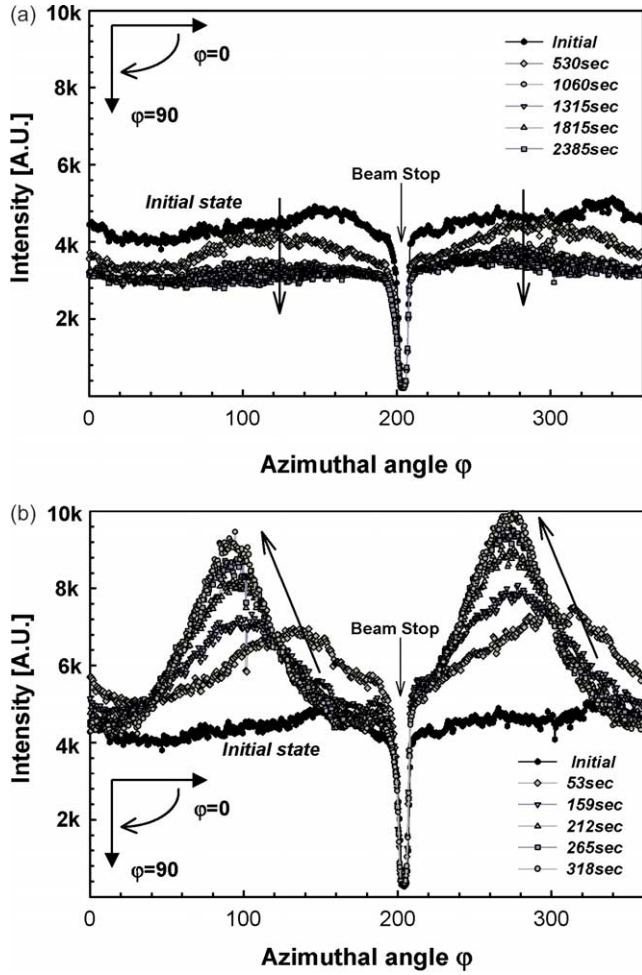
Fig. 8. Azimuthal scan of in situ 2D SAXS images under (a) AC field and (b) DC field.

kinetics of the reaction can be described as follows

$$\frac{dx}{dt} = k(x_i - x), \tag{2}$$

where x_i is its equilibration value and k is the kinetic constant, which is a function of the electric field. The integration of Eq. (2) with the initial condition of $x(0) = x_0$ yields

$$x = x_i + (x_0 - x_i)e^{-kt}. \tag{3}$$

It is reasonable that k and x_i are functions of the electric field strength. If x_i, which is the degree of evolution in the alignment at a given DC field, is assumed to be a perfect orientation, it must be independent of the DC field strength. It is also reasonable to assume that the increase in the storage modulus is a function of x

$$\Delta G' = f(x,E). \tag{4}$$

where $\Delta G' = G'(t) - G'_0$ is the increase in the storage modulus at time t and E is the electric field strength. Because x and $\Delta G'$ have different physical quantities with different units, the function $f(x)$ must be scaled by a certain factor, which can be

replaced by $\Delta G'_\infty$, giving the following equation

$$\Delta G' = \Delta G'_\infty \tilde{f}(x;E) \tag{5}$$

where the function $\tilde{f}(x;E)$ is a dimensionless function of x. The theory of dimensional analysis such as the Π-theorem shows that the dimensionless dependent variable is a dimensionless function of dimensionless independent variables [25]. A candidate for the dimensionless independent variable may be the following normalized structure variable

$$\tilde{x} = \frac{x(t,E) - x(0,E)}{x(\infty,E) - x(0,E)} = \frac{x - x_0}{x_i - x_0} = 1 - e^{-kt} \tag{6}$$

Combining Eqs. (5) and (6) leads the following equation

$$\tilde{G}' = \frac{\Delta G'}{\Delta G'_\infty} = \tilde{f}(\tilde{x}) \tag{7}$$

The above reasoning explains why Eq. (1) describes the experimental data well. However, it should be noted that the x of DC and that of AC are totally different quantities, which was checked with SAXS experiments. The validity of TES (Fig. 3) irrespective of the field type (AC and DC) suggests that the x of DC and that of AC share the same functional structure. This means that

$$\tilde{f}_{AC}(x_{AC}) = \tilde{f}_{DC}(x_{DC}) \text{ whenever } x_{AC} = x_{DC}. \tag{8}$$

However, it is difficult to find appropriate conditions for Eq. (8) to hold.

The dimensionless function $\tilde{f}(x)$ must satisfy the following conditions. Because the normalized variables ($\tilde{x}$ and $\tilde{G}'$) are increasing functions of time and must be between zero and unity, we have

$$\tilde{f}(0) = 0, \quad \tilde{f}(1) = 1 \quad \text{and} \quad \frac{d\tilde{f}}{d\tilde{x}} \geq 0 \tag{9}$$

The simplest form of $\tilde{f}(x)$ is

$$\tilde{f}(\tilde{x}) = \tilde{x} \tag{10}$$

Eq. (10) is another form of Eq. (1) with $k = 1/\lambda$. The validity of Eq. (1) in both AC and DC fields suggests that the normalized modulus $\tilde{G}'$ is simply a dimensionless structural variable.

In addition, it should be noted that the characteristic time, t_s of ER (Electro-Rheological) fluids [26] scales

$$t_s \propto \frac{\eta_s}{E^2}, \tag{11}$$

where η_s is the medium viscosity of ER fluids and E is the strength of the electric field. The mechanism of an ER fluid is known as the alignment of ER particles to the field direction as a result of polarization. This scaling behavior of ER fluids agrees with that shown in Fig. 4 (DC case), which adds another evidence that the clays align with the field direction under DC field in our nanocomposite system.

It is also interesting to note that DC does not induce exfoliation where AC does. Polymer/clay nanocomposites can be considered as polarizable particles (clay) embedded in a dielectric medium (polymer). A dipole will be induced on
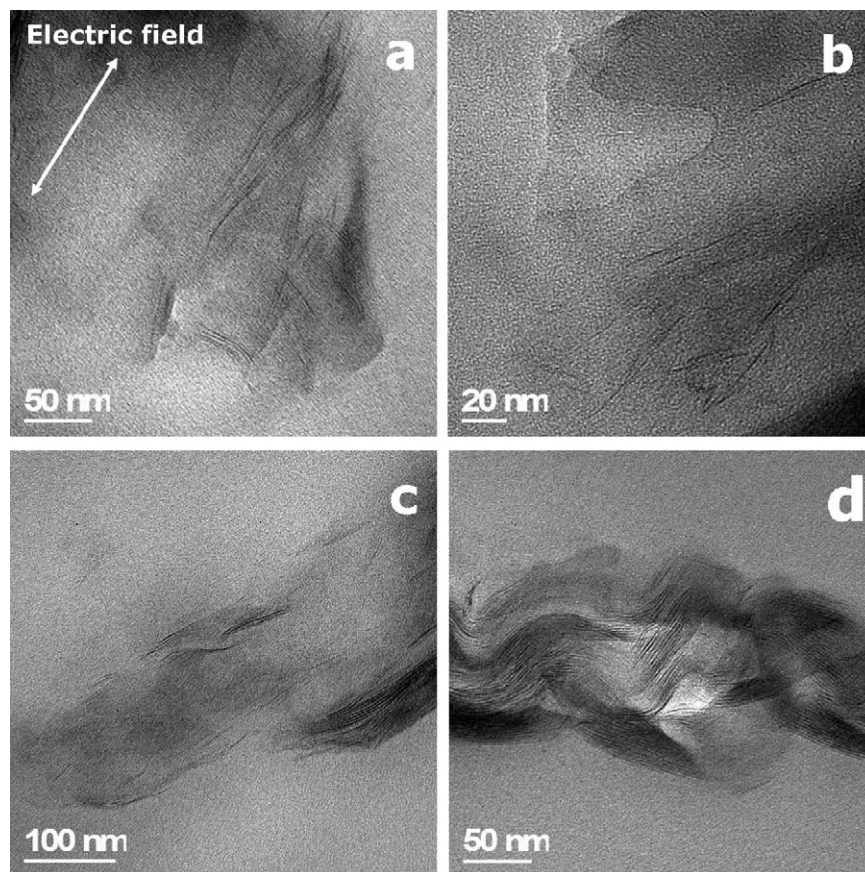
Fig. 9. TEM images of PP/clay nanocomposite before (d) and after (a)–(c) AC application (1 kV/mm–60 Hz, 3300 s).

the particles when an electric field is applied to these systems, both AC and DC. The clay used in this study, which are members of the mica family, consists of anionic aluminosilicate layers separated by a regular van der Waals gap (gallery) containing charge-balancing exchangeable cations. When the electric field is applied, the interlayer surfactants in the vicinity of the layer surface tends to move back and forward to induce the effective polarizability of the particles resulting in an induced dipole on the clay layers or tactoids [27]. This mobility of the surfactants along the layer surface can arise from the diffusive electrostatic potential between the surfactants and silicate layers over several oxygen atoms [28,29]. Under DC field, the mobile cationic surfactants move toward the layer edge inducing a dipole in the direction parallel to the layer axis. This is because the structural anisotropy of the clays causes a stronger dipole moment in the direction parallel than in the direction perpendicular to electric field. Therefore, the clay needs to be aligned along the direction of the electric field by a rotation of the clay tactoids (dielectrophoretic motion). Recently, the alignment of nanoparticles such as clays or carbon nanotubes under electric field (AC and DC) has been reported [29–36]. They showed that the electric field, either AC or DC, induces a dipole on the particles resulting in dielectrophoretic motion, which leads to the alignment structure in a slightly different manner according to the field type. However, they used a low-viscosity matrix such as an epoxy monomer or alcohol. Dielectrophoretic motion is restricted in a high-viscosity matrix. It is difficult to expect the rapid re-arrangement of the surfactant configurations with rapidly changing electric fields in high-viscosity matrix. The restriction not only hinders the motion of the surfactants and the layers, but also gradually detaches the surfactants from the layer.

In case of DC field, orientation of clay particles occurs, because electric field keeps a fixed direction for sufficiently long time that slow motion of surfactant due to high viscosity results in the orientation of clay particles. On the other hand, AC field varying field direction does not give enough time for slow motion of surfactant to form the aligned structure of clay particles. It is noticeable that slow motion of the surfactants (cations) implies movement of surfactants to reduce total electrostatic energy of clay under field. The motion is not random but similar to the drift motion of ions under electrical field. There is another mode of motions of surfactants that is random and like diffusion. The work done by AC field on surfactants become dissipative to increase the amplitude of the random motion. Increase of the random motion possibly destroys balance of van der Waals interactions and electrostatic interactions Balance of the interactions maintains stacking of silicate layers, because repulsions between anionic layers are cancelled by the attraction due to surfactant cations and van der Waals interaction. Thus, we can guess that the increase of the random motion breaks the balance of the interactions by charge unbalance, which is triggered by a surfactant molecules
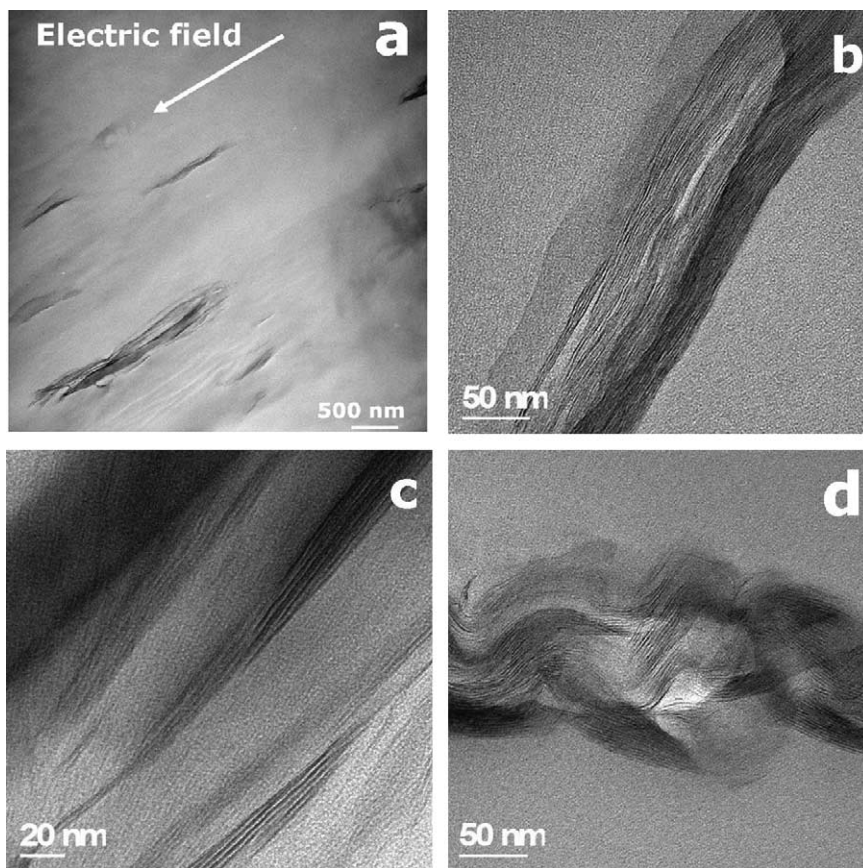
Fig. 10. TEM images of PP/clay nanocomposite before (d) and after (a)–(c) DC application (1 kV/mm, 1000 s).

separated from the neighbour of stacks of silicate layers. In order to check this reasoning, we performed a dielectric relaxation analysis.

Table 1 shows the measured dielectric properties. Electric conductivity was calculated from the equation $\sigma = \varepsilon'' \omega \varepsilon_0$ where the terms on the right hand side are measured imaginary part of the dielectric constant, frequency, and permittivity in the free space, respectively. Dielectric relaxation spectrum needs to be transformed to remove the effect of electrode polarization term ($\varepsilon' = \varepsilon'_{relax} + \varepsilon'_{el}$) and the effect from DC conductivity ($\varepsilon'' = \varepsilon''_{relax} + \varepsilon''_{dc}$). The details of the dielectric relaxation analysis are outside the scope of this paper and will be reported later. In this paper, only the electrical conductivity and the number of bound ions will be provided. The electric conductivity of HP is in the order of 10^{-12}–10^{-9} S/cm, which is typical for an insulator. The electric conductivities of HPC, HPCA and HPCD are in the range of 10^{-11}–10^{-7} S/cm, i.e. 1–2 orders of magnitude higher than that of HP. This suggests that the PP with clay has a large number of charge carriers that contribute to the electric conductivity. These carriers would be surfactant ions originating from the clays. Ions in the PP-clay nanocomposites can be divided into two types according to the mobility of the ions; bound ions (cationic surfactants on the clay surface) and free ions (cationic surfactants in the PP matrix). The number density of the bound ions (N_b) shown in Table 1 explains the behavior of the surfactants under AC field. N_b can be obtained from dielectric relaxation analysis using the equation,

$N_b \propto \varepsilon_0 \Delta\varepsilon/\tau_0$, where $\Delta\varepsilon \equiv \varepsilon'_0 - \varepsilon'_\infty$. Details of the dielectric relaxation analysis will be reported elsewhere. Table 1 shows that the N_b of HPCA is much smaller than those of HPC and HPCD, which suggests the transformation of bound ions into free ions due to the detachment of the bound ions in the presence of AC field. This detachment of the cationic surfactant causes an unbalance in the electrostatic forces between the anionic aluminosilicate and the cationic surfactant. When the electrostatic repulsive force overcomes the attractive van der Waals force between the layers, they repel each other resulting in the destruction of layer-stacking. On the other hand, the N_b of HPCD does not change, which suggests that the electrostatic balance does not vary significantly under DC field because the DC field does not change its direction and strength. Therefore, the restriction of surfactant motion does not have an adverse

Table 1

Electric conductivity and dielectric properties of PP and PP/clay melts with and without electric fields

Samples[a]	$\sigma_{0.1}$ (S/cm)[b]	$\sigma_{100\,k}$ (S/cm)[c]	$\varepsilon_0\Delta\varepsilon/\tau_0$ ($\times 10^{-9}$ S/m)[d]
HP	3.38×10^{-12}	9.69×10^{-9}	–
HPC	1.07×10^{-11}	2.54×10^{-7}	50.6
HPCA	1.39×10^{-11}	3.58×10^{-7}	12.0
HPCD	1.68×10^{-11}	3.01×10^{-7}	49.0

[a] Abbreviation of samples.
[b] Electric conductivity at 0.1 Hz.
[c] Electric conductivity at 100 kHz.
[d] Number of bound ions.

effect on the orientation of the clay particles. This is because the surfactants move together with the layer-stacks.

In summary, we investigated the effect of electric field on the nanostructure of PP/clay nanocomposites. The morphological evolution of nanocomposites under electric field strongly depends on the exposure time as well as on the electric field strength. TES shows a universal relationship between the exposure time and the electric field. Furthermore, parameter analysis shows different phenomena according to the electric field types. This was confirmed by SAXS patterns and TEM images, which shows that these differences arise from the different morphological evolution under electric field according to the field type. AC field induces the exfoliation structure while DC field aligns the clays. The validity of TES and two distinct microstructural evolution mechanisms according to the type of electric fields were also discussed. The alignment process due to dielectrophoretic motion was confirmed by comparing with the electro-rheological (ER) phenomena. In addition, dielectric relaxation analysis showed that the exfoliation process was due to an unbalance between the van der Waals interaction and the electrostatic interactions.

4. Conclusions

The electric fields were applied to PP/clay nanocomposites in order to regulate the microstructure. The difference and similarity between the effects of AC and DC fields on the nanocomposites were investigated using rheology, in situ SAXS, TEM and dielectric relaxation measurements. The enhanced G' under electric fields, either AC or DC, were successfully predicted using Eq. (1) irrespective of the field type, while parameter analysis from Eq. (1) showed differences between AC and DC fields. G'_i/G'_0 increased with time in different ways according to the field types. The characteristic time, λ, also showed a different dependence on the field strength. These differences are believed to be due to the distinct structural characteristics, which were evaluated by SAXS with the support of TEM. In an AC field, the isotropic ring loses its brightness with time, which suggests an exfoliation process. It was difficult to observe any alignment process from the scattering pattern. However, in the case of DC, there was a strong tendency of alignment and no loss of brightness. Eq. (8) suggests that the validity of TES can be ascribed to the underlying functional structure reflected on G' in the AC and DC fields, which was confirmed experimentally.

Two different microstructural evolution mechanisms in PP/clay composites under the electric fields were also examined using dielectric relaxation analysis, which showed that the dielectrophoretic motion of the clays arising from a DC-induced dipole leads to an alignment structure, and charge imbalance resulting from the detachment of the surfactants on the clay surface under AC field results in an exfoliated structure (or layer-stacking destruction).

References

[1] Messersmith PB, Giannelis EP. J Polym Sci A: Polym Chem 1995;33: 1047.
[2] Porter D, Metcalfe E, Thomas MJK. Fire Mater 2000;24:45.
[3] Giannelis EP. Adv Mater 1996;8:29.
[4] Messersmith PB, Giannelis EP. Chem Mater 1993;5:1064.
[5] Messersmith PB, Giannelis EP. Chem Mater 1994;6:1719.
[6] Wang MS, Pinnavaia TJ. Chem Mater 1994;6:468.
[7] Lan T, Pinnavaia TJ. Chem Mater 1994;6:2216.
[8] Aranda P, Ruiz-Hitzky E. Adv Mater 1990;2:545.
[9] Wu J, Lerner M. Chem Mater 1993;5:835.
[10] Vaia RA, Ishii H, Giannelis EP. Chem Mater 1993;5:1694.
[11] Vaia RA, Vasudevan S, Krawiec W, Scanlon LG, Giannelis EP. Adv Mater 1995;7:154.
[12] Kawasumi M, Hasegawa N, Kato M, Usuki A, Okada A. Macromolecules 1997;30:6333.
[13] Kim DH, Park JU, Ahn KH, Lee SJ. Macromol Rapid Commun 2003; 24:388.
[14] Krishnamoorti R, Vaia RA, Giannelis EP. Chem Mater 1996;8:1728.
[15] Ren J, Silver AS, Krishnamoorti R. Macromolecules 2000;33:3739.
[16] Solomon MJ, Almusallam AS, Seefeldt KF, Somwangthanaroj A, Varadan P. Macromolecules 2001;34:1864.
[17] Krishnamoorti R, Yurekli K. Curr Opin Colloid Interface Sci 2001;6: 464.
[18] Potschke P, Fornes TD, Paul DR. Polymer 2002;43:3247.
[19] Mitchell CA, Bahr JL, Arepalli S, Tour JM, Krishnamoorti R. Macromolecules 2002;35:8825.
[20] Krishnamoorti R, Giannelis EP. Macromolecules 1997;30:4097.
[21] Lim YT, Park OO. Macromol Rapid Commun 2000;21:231.
[22] Pattamaprom C, Larson RG, Van Dyke TJ. Rheol Acta 2000;39:517.
[23] Cho KS, Ahn KH, Lee SJ. J Polym Sci B: Polym Phys 2004;42:2730.
[24] Trappe V, Weitz D. Phys Rev Lett 2000;85:449.
[25] Barenblatt GI. Scaling, self-similarity, and intermediate asymptotics. New York: Cambridge University Press; 1996.
[26] Larson RG. The structure and rheology of complex fluids. New York: Oxford university press; 1999 [chapter 8].
[27] Ishida T. Encyclopedia of surface and colloid science, vol. 4. New York: Marcel Dekker, Inc.; 2002 p. 1385–1392.
[28] Bleam WF, Hoffman R. Inorg Chem 1988;27:3180.
[29] Koerner H, Jacobs D, Tomlin DW, Busbee JD, Vaia RD. Adv Mater 2004; 16:297.
[30] Yamamoto K, Akita S, Nakayama Y. J Phys D: Appl Phys 1998;31:34.
[31] Chen XQ, Saito T, Yamada H, Matsushige K. Appl Phys Lett 2001; 78:3714.
[32] Martin CA, Sandler JKW, Windle AH, Schwarz MK, Bauhofer W, Schulte K, et al. Polymer 2005;46:877.
[33] Kim JW, Kim SG, Choi HJ, Jhon MS. Macromol Rapid Commun 1999; 20:450.
[34] Sung JH, Choi HJ. Korea-Australia Rheol J 2004;16:193.
[35] Lin-Gibson S, Kim H, Schmidt G, Han CC, Hobbie EK. J Colloid Interface Sci 2004;274:515.
[36] Lin-Gibson S, Schmidt G, Kim H, Han CC, Hobbie EK. J Chem Phys 2003;119:8080.